Fast NIR-Single-Pixel-Imaging enhancement under scattering environment

Carlos A. Osorio Quero*, Daniel Durini, Jose Rangel-Magdaleno, Jose Martinez-Carranza and Ruben Ramos-Garcia
Instituto Nacional de Astrofísica, Óptica y Electrónica (INAOE), 72840, Mexico.

ABSTRACT

The captured images in scattering scenarios are a challenge to solve for the vision systems for Unmanned Flight Vehicles (UFVs). Currently, research has been conducted on the use of sensors in the near-infrared (NIR) part of the spectra as an option for the RGB camera in scenarios with higher scattering (fog or rain), because to the diameter of water particles is proportional to the wavelength, then Mie scattering occurs with that the transmittance is higher. Therefore, in this work, we present a solution vision system based on single-pixel imaging at the wavelength of 1550 nm (NIR-SPI) to capture 2D images in a scattering environment (Fog and Rain). For which we evaluate the performance of the 2D image reconstruction in controlled laboratory settings using different compressive sensing (CS), Fourier single-pixel imaging (FSI), and Hadamard-single-pixel-imaging (HSI) reconstruction methods fused with dark channel prior (DCP) dehazing methods to improve 2D image quality. This work will determine which strategy of processing and imaging is more suitable in terms of quality image (EPI), entropy and contrast, and processing time to suit the Unmanned Flight Vehicles (UFVs).

1 INTRODUCTION

In the last year, the use the Unmanned Flight Vehicles (UFVs) increase, covering different applications in outdoor environments as infrastructure inspection [1], rescue operations [2], and surveillance [3]. For which is needs to be captured image under different conditions, light and weather. However, bad weather images captured show some degradation effects such as blurriness and low contrast. Due to light traveling through a medium that contains suspended water-particles, it is exponentially attenuated through two processes: absorption and scattering [4]. Being difficult to distinguish objects in the environment. In such scenarios, the performance of the vision system based on RGB (Red-Green-Blue) is limited, in the visible spectrum we meet in the Rayleigh regime [5] with a D diameter water-particles is $D << \lambda$, where λ is the wavelength , in this case the attenuation the light is highest decreases the contrast level , while for wavelength Near-infrared (NIR) $D \sim \lambda$ is in the Mie regime [6], where the effects of the light attenuation and scattering are fewer in comprised with the visible spectrum, being the use of NIR sensor a solution for increase performance vision systems of the UFVs [7].

Therefore, the solution proposed in this work is a system vision on NIR based on a Single-Pixel Camera (SPC) [8], an architecture that uses a single detector as an alternative to the traditional cameras that capture the scene directly using a sensor array (see Fig. 1), and has these two essential advantages: (i) it provides the means to acquire the image in the compressed form, reducing the processing time; and (ii) it is suitable to perform imaging to different wavelengths, with that we can take advantage from a wider part of the electromagnetic spectrum, which is ideal for application with UFV. This system allows capturing the image in the NIR spectrum, where the attenuation environment is the lowest visible, and the image obtained can be enhanced through of used Dark Channel Prior (DCP) method [9]. From background light (BL) estimation and transmission map (TM) over image, single-pixel imaging (SPI) is possible to refine the image by removing the hazy effects in the image.

To summarize, the main contributions and limitations of this paper are as follows:

- We developed a SPC NIR-SPI with active illumination at a wavelength of 1550 nm with a resolution size of 8x8 and implement three type reconstruction algorithms based on compressive sensing (CS), Fourier single-pixel imaging (FSI), and Hadamard-single-pixel-imaging (HSI).

- Implementation the Dark Channel Prior (DCP) method over images SPI and evaluation of laboratory the NIR-SPI system in the test chamber.

- Evaluation of the CS, FSI, and HSI methods 2D reconstruction of SPI in a simulated environment applying the proposed DCP algorithm, in terms of Edge Preservation Index EPI [10], and processing time. To determine which method best adapts the conditions, of the scattering environment.

*Email address(es): caoq@inaoep.mx

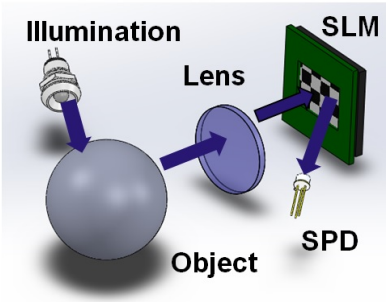

Figure 1: Schematic generation single-pixel imaging:the object illuminated by a light source and the light reflected by it gets directed through a lens onto an SLM, where is capture by the SPD [7].

2 SINGLE-PIXEL IMAGING (SPI) 2D RECONSTRUCTION

Single-pixel imaging is based on the projection of spatially structured light patterns by using light modulation devices such as: (i) Spatial light modulators (SLM) that allow light to be modulated in terms of amplitude, phase, or wave polarization in space and time, (iii) Digital micromirror devices (DMD) that operate as digital on/off modulators of the reflected light on the micromirror array, through the change of the tilt angle it is possible to reflect or obstruct light projecting a light pattern modulate over the scene, (iii) LED matrix as light digital on/off modulation, that allow faster changes the light patterns than SLM and DMD devices. The reflected light is focused on a photodetector with no spatial information S_i (see Fig. 1). From the correlations between the patterns $\Phi_i(x,y)$ and S_i, we can reconstructed the image $O,(x,y)$, where the reconstructed image is obtained as the product of the measured single S_i and the corresponding structured pattern that originated defined by Eq. (1) [11].

$$O\,(x,y) = \alpha \sum_{x=1}^{M}\sum_{y=1}^{N} S_i \Phi_i\,(x,y) \tag{1}$$

For reconstruction SPI, we can apply different as compressive sensing (CS), Fourier single-pixel imaging (FSI), and Hadamard-single-pixel-imaging (HSI) methods, which use transformations or iterative algorithms [8]. In FSI and HSI, both acquire the spectrum, the object image and reconstruct the object image by applying an inverse transform. For FSI, the sinusoidal patterns (see Fig. 2b), defined by Eq. (2) [12].

$$\Phi_{iFSI}(x,y) = a + b \cdot cos(2\pi x + 2\pi y + \phi) \tag{2}$$

$$R(u,v)_{FSI} = [R_0(u,v) - R_\pi(u,v)] + j[R_{\pi/2}(u,v) - R_{3\pi/2}(u,v)] \tag{3}$$

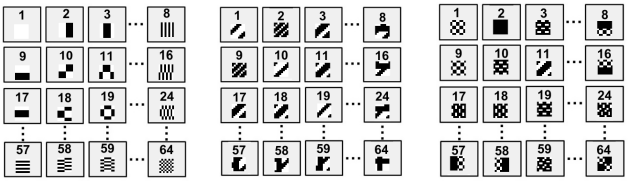

Figure 2: Patterns SPI: a) Hadamard patterns basic [7], b) FSI patterns [12], c) HSI patterns [8].

Where the variable a is the average pattern intensity and the variable b is the contrast [12]. The projection of the FSI patterns varies with the phases ($\phi = 0, \phi = \pi/2, \phi = \pi, \phi = 3\pi/2$). We can obtain a value of intensity light over a detector with a spectrum of the object $R(u,v)_{FSI}$ expressed by Eq. (3). The object image $O_{FSI}(x,y)$ can then be reconstructed by applying the IFT2 $O_{FSI}(x,y) = F^{-1}(R(u,v)_{FSI})$.

For HSI, we used the Hadamard patterns Eq. (4) (see Fig. 2c), from the patterns projected over the object can obtain differential measurement $R(u,v)$ and the reconstruction object $O_{HSI}(x,y)$ can be obtained using an inverse Hadamard transform $O_{HSI}(x,y) = H^{-1}(R(u,v))$ [12]. To implementation the FSI and HSI patterns in DMD or LED array is must apply dither algorithm to generate binary patterns, that they can be adapt theses technologies [13].

$$\Phi_{iHSI}(x,y) = \tfrac{1}{2}(1 + H^{-1}\delta^{th}(u,v)) \qquad \delta^{th}(u,v) = \begin{cases} 1, u = u_0, v = v_0 \\ 0, otherwise \end{cases} \tag{4}$$

In the case of the CS method, the generate the Hadamard pattern Φ_i based on Sylvester's recursive matrix generation principle [8] (see Fig. 2a). For reconstruction, apply CS, we use an iterative method based on (Orthogonal Matching Pursuit) OMP-GPU [14], where it needs to Hadamard pattern Φ_i and measurements.

3 BACKGROUND

When light interacts with water-particles, various physical phenomena occur such as: reflection, refraction, absorption, and scattering. The scattering is related to the particle size (sp), and its cross-section Q_d [7], where $sp = \pi D/\lambda$, D is the particle diameter, and λ the incident photon wavelength. For small scattering particles with $D << \lambda$, the distribution of scattered light is symmetric in the forward and backward directions (Rayleigh regime). If the particle size increases, the scattered energy increases toward the incident beam, reducing the amount of scattered light in the opposite direction (Mie regime).

3.1 Atmospheric scattering model

The image received by a sensor from scene points is often absorbed and scattered by the medium. Therefore, an image can be defined using McCartney's atmospheric scattering model using Eq. (5) [15].

$$I(x,y) = J(x,y)TM(x,y) + BL(x,y)(1 - TM(x,y)) + n(x,y) \quad (5)$$

Where I (x, y) denotes the observed degraded image. J (x, y) denotes the scene radiance, which represents the original appearance of image BL (x, y), the global atmospheric light, and TM (x, y) is the atmospheric transmission map defined by Beer-Lambert-Bouguet law as $TM(x,y) = e^{-\beta \hat{L}}$, $-\beta$ is the extinction coefficient [9]. The term, J(x,y)TM(x,y) is called the direct attenuation indication, of the decay of the scene radiance in the medium. BL (x,y)(1-TM(x,y)) is the airlight increases as the scene depth increases, and n (x, y) denotes zero-mean Gaussian noise from the environment and sensor.

3.2 Dehazing Image

In the DCP-based dehazing algorithm [9]. For applying DCP algorithm there are six steps: (i) airlight estimation (BL), (ii) dark channel estimation $J(x,y)$, (iii) coarse transmission estimation (TM), (iv) transmission refinement, (v) scene recovery, and (vi) image equalization (see Fig. 3).

- **Airlight estimation (BL):** Obtained from defined over image $(I(x,y)^{dark})$ a local patch or area, where local entropy is measured for estimation BL Eq. (6) [9]. The local entropy value is low for regions with smooth variations, which correspond to haze-opaque regions (zone with scattering)

$$BL(x,y) = I(argmax_{x,y}(I(x,y)^{dark})) \quad (6)$$

- **Dark channel estimation:** The dark channel is first constructed from the input image J, the estimation of the dark channel is shown in Eq. (7), where J^c represents the color channel of J and $\Omega\ (x,y)$ is local path anchored, the value $J^{dark}(x,y)$ is low and tends to be zero except for the sky region [9]. The transmission in a local path $\Omega(x,y)$ is assumed to be a constant.

$$J^{dark}(x,y) = \min_{y \in \Omega(x,y)} \left(\min_{c \in \Omega(r,g,b)} J^c \right) \quad (7)$$

- **Coarse transmission estimation (TM):** The Eq. (8) [9], with a control parameter ω= 0.95, The luminance-based transmission map $TM(x,y) = e^{-\beta \hat{L}}$, $\hat{L}$ denoting the modified luminance value define as $\hat{L} = \frac{\tau}{L^*} L(x,y)$, where L(x,y) is the luminance of the input image I(x,y), τ is the depth range , and L^* denote a percentage of the luminance L(x,y) .

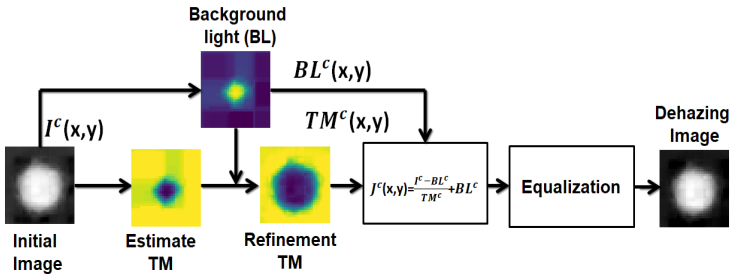

Figure 3: Overall block diagram Dark Channel Prior (DCP) method applying on single-pixel foggy environment [9].

$$TM(x,y) = 1 - \omega \min_{y \in \Omega(x,y)} \left(min \frac{I^c}{BL^c} \right) \quad (8)$$

- **Transmission refinement:** Incorrect estimation of the transmission map can lead to problems such as false texture and blocking artifacts. To improve the accuracy of the transmission map, there are methods such as Gaussian, Bilateral, Guided or Cross-bilateral filters and soft matting using minimizing energy function [9].

- **Scene recovery:** The atmospheric light and the transmission map are then obtained from the dark channel. The transmission map is further refined, and the haze-free image is finally reconstructed as Eq. (9) [9].

$$J(x,y) = \frac{I(x,y) - BL(x,y)}{max(TM(x,y), t_{th})} + BL(x,y) - \frac{n(x,y)}{TM(x,y)} \quad (9)$$

- **Image equalization:** The image recovery is equalized improvement the level contrast the new image.

For the implementation of the DCP algorithm on GPU over images SPI, we proposed the reducing computational complexity of implementation fast guided filter by transmission refinement, using the strategy of comparison score value with threshold θ_{th} score=mean(I(x,y))-var(I(x,y))$> \theta_{th}$ for air-light estimation.

4 NIR-SPI SYSTEM

The NIR-SPI vision system using structured illumination, which improves image quality in the presence of strong backlight and stray light (see Fig. 1), provided by an array of 8 x 8 NIR-LEDs emitting radiation with a peak wavelength of 1550 nm. The SPD used is an InGaAs photodiode. This active illumination approach offers several advantages, as it

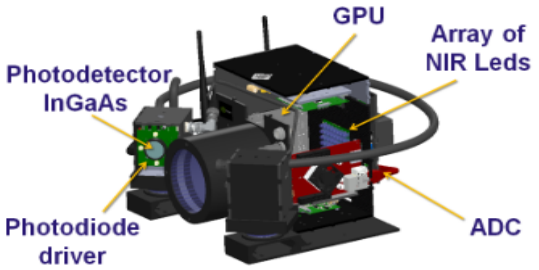

Figure 4: Proposed Single-Pixel Camera (SPC) dimension 11 x 12 x 13 cm, focal length 20 cm, weight 1.3 kg, power consumption 25 W, module photodiode, active illumination source, photodetector diode InGaAs FGA015 GPU unit and ADC [7].

can operate in different outdoor weather under low-level illumination (scenarios with dust, fog, rain, or smoke) and it is less sensitive to background radiation noise [7]. The NIR-SPI architecture proposed in this work is divided into two main parts: (i) the basic elements used to generate images through the single-pixel principle: an InGaAs photodetector (diode FGA015 @ 1550 nm), an array of emitting NIR-LEDs, and an ADC (see Fig. 4), and (ii) the subsystem in charge of processing the electrical output signal provided by the SPD module, digitized using the ADC, and the respective data processing using a Graphics Processing Unit (GPU) (see Fig. 4). The GPU unit (Jetson-Nano) is responsible for generating the Hadamard patterns and processing the converted data by the ADC, used by the Batch-OMP Algorithm [14] running in the GPU unit to generate the 2D images.

5 Experimental Results

To evaluate the Single-Pixel Camera (SPC) capabilities with active illumination using the different projection methods, we developed a testing bench that has a controlled system illumination to simulate background outdoor light and a system that can simulate the conditions of scattering environment. As test objects, we used rocks and pine seeds (see Fig. 6- Fig.7) to emulate a forest environment an explore capability capture of NIR image. In the tests, we defined a scenario foggy (water-particles diameter 3μm [7]), and levels of illumination 15 Klux (half-cloudy)-30 Klux (midday) [7], where the object test is at distance 60 cm. For reconstructing the 2D image applying the CS, FSI and HSI methods under the two light conditions. The 2D SPI image (see Fig. 6) is improved applying the DCP method (see Fig. 7- 8), as evaluation parameters of the final reconstructed images, we calculated the corresponding EPI [10], setting the goal parameters as EPI $>$ 0.5 (see Tab. 1), and time processing (see Tab. 2).

5.1 Discussion: Testing 2D NIR-SPI enhancement image

In the tests carried out to a 2D image reconstruction in a scattering environment applying the FSI, HSI, and CS methods at a measured distance 60 cm with illumination conditions of midday (see Fig. 6), and half-cloudy (see Fig. 8a). In the first test, with illumination conditions midday, we applied the DCP algorithm and obtained values of EPI $>$ 0.5 (see Table. 1) for the cases of HSI and CS with processing times between 41 and 47 ms (see Table. 2). For FSI observed a processing time fewer, with a value of EPI $<$ 0.5 showing low-capacities reconstruction and high sensitivity in scattering scenarios. In the second test, we changed the scenario by reducing the level of illumination (half-cloudy) for this scenario the contrast of the image reconstructed is reduced (see Fig. 8) , then applying the DCP algorithm, shows its high capacities for improving image quality obtained values of EPI $>$ 0.7 (see Table. 1) being the CS method the best with a processing time of 39 ms (see Table. 2), although in the case FSI presents a processing time, the image quality is the lowest. In terms of image quality, we can see improvement in the contrast level and a reduction in the entropy H_e applying the DCP algorithm (see Table. 3) in the SPI methods obtained, similar values contrast with variations in the entropy (the entropy affected the smoothing in the images) being the HSI method with H_e lowest.

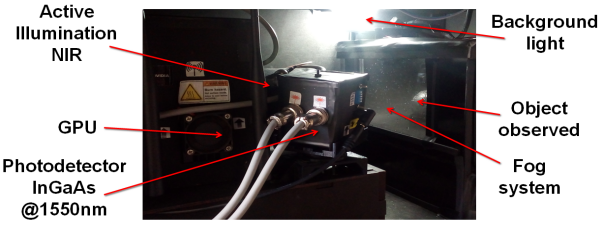

Figure 5: Experimental setup to vision system 3D NIR-SPI, the testing bench for simulate scattering environment [7].

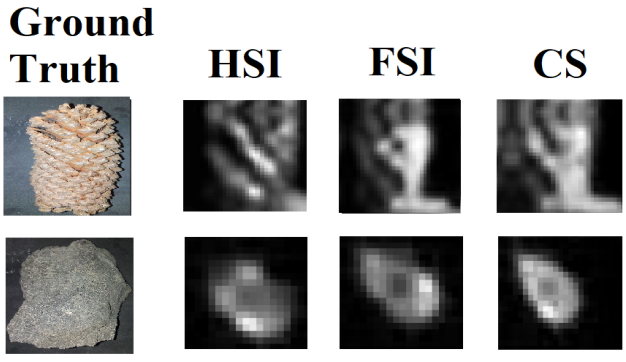

Figure 6: Reconstruction 2D NIR-SPI a scenario of foggy and midday using HSI, FSI, and CS methods.

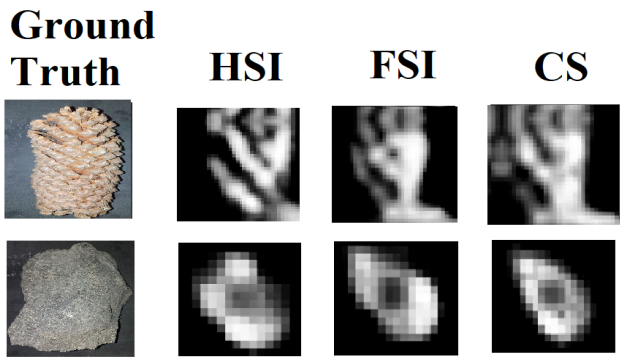

Figure 7: Reconstruction 2D NIR-SPI a scenario of foggy and midday using HSI, FSI, and CS methods applying DCP algorithm.

Table 1: EPI noise suppression applying DCP for the case a scenario with a foggy and background illumination of 15 KLux (half-cloudy)- 30 KLux (midday).

SPI method	EPI_{30KLux}	EPI_{15KLux}
CS	0.65	0.8
FSI	0.47	0.74
HSI	0.51	0.76

6 NIR SPI 2D IMAGE RECONSTRUCTION APPLIED TO UAVS AUTONOMOUS NAVIGATION IN OUTDOOR CONDITIONS

A vision system that operates in fog conditions is an advantage in Unmanned Aerial Vehicle (UAV) navigation applications. It provides fast deployment at remote or challenging locations, being essential for many civil and military applications such as post-disaster relief assistance [2]. Our NIR-SPI system developed, if adopted in UAVs (see Fig. 9), offers a solution to perform better visualization of the scene in outdoor conduction, if compared to conventional vision systems that normally use RGB sensors operating in the visible spectrum [7]. As explained, conventional systems operating in the VIS range present much higher image degradation in fog conditions than those operating in the NIR part of the spectra [7]. In the literature, there are examples of the use of IR vision systems to UAVs for applications such as rescue missions that enable fast exploration in scenes with low-illumination, or operations performed in complex weather conditions that limit the drone visibility. NIR-SPI system presented has great potential to be used in similar applications. Furthermore, SPI could be an alternative to the use of LIDAR technology.

7 CONCLUSIONS

This paper presented an evaluation of the HSI, FSI, and CS methods in a combination with the DCP algorithm as a strategy to improve image quality in a scattering environment

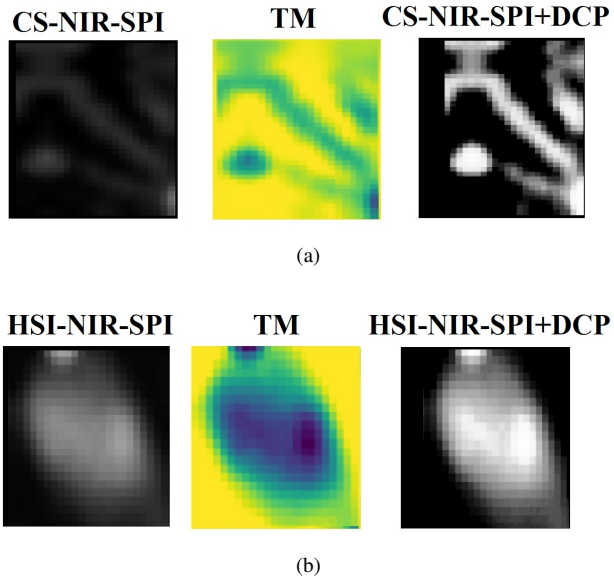

Figure 8: Reconstruction 2D NIR-SPI a scenario of foggy and half-cloudy using HSI and CS, in this scenario the 2D image NIR-SPI present low-contrast, obtained the TM and applying the DCP algorithm: a) pine seeds, and b) rock.

Table 2: Processing time 2D NIR-SPI DCP for the case a scenario with a foggy and background illumination of 15 KLux (half-cloudy)- 30 KLux (midday).

SPI method	$T_{30KLux}(ms)$	$T_{15KLux}(ms)$
CS	41	39
FSI	37	35
HSI	44	41

with different illuminations for a vision system SPC with active illumination for future use as a vision system in UFV. As test objects used rocks and pine seed elements in the forest environment. For the test, we generated foggy artificial and two illumination conditions half-cloudy and midday, in this simulated scenario presents a challenge to make good detection of the image, due to the attenuation effect caused by interacting the light with water particles. To improve the SPI image, we applied a DCP algorithm to the reconstructed image. In the case of the FSI, the SPI image reconstructed is more sensitive to source noise, an effect that we can observe in the evaluation of the term EPI (see Table. 1), and contrast (see Table. 3). For which is not recommended in SPI vision systems under scattering conditions. In the test, HSI and CS methods were shown to be robust under scattering conditions (see Table. 1) , mainly in the case low-contrast of the SPI image (see Fig. 8), being ideal to use as SPI reconstruction methods applied in the SPC. This capture capacity of SPI images under the scattering scenario shows the feasibility of using a vision system based on the SPI principle for applications to vehicles

Table 3: Improvement the 2D NIR-SPI in terms entropy H_e, and contrast (C) applying DCP algorithm.

SPI method	H_e	C	H_{eDCP}	C_{DCP}
CS	7.39	10	6.3	11
FSI	7	9	5.3	9.8
HSI	6.74	9.95	5.2	10

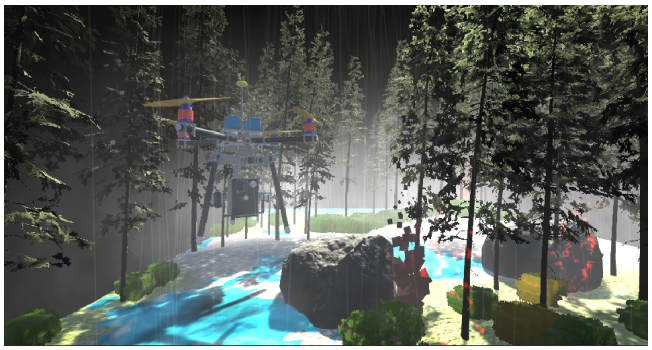

Figure 9: Schematic view to illustrate UAV (drone) navigation in presence of fog.

UFV as a redundant sensor vision for the RGB cameras.

ACKNOWLEDGEMENTS

The first author is thankful to Consejo Nacional de Ciencia y Tecnología (CONACYT) for his scholarship with No. CVU: 661331.

REFERENCES

[1] Ioannis Pitas. Drone vision and deep learning for infrastructure inspection. In *2021 IEEE International Conference on Autonomous Systems (ICAS)*, pages 1–1, 2021.

[2] Yogianandh Naidoo, Riaan Stopforth, and Glen Bright. Development of an uav for search amp; rescue applications. In *IEEE Africon '11*, pages 1–6, 2011.

[3] Zainab Zaheer, Atiya Usmani, Ekram Khan, and Mohammed A. Qadeer. Aerial surveillance system using uav. In *2016 Thirteenth International Conference on Wireless and Optical Communications Networks (WOCN)*, pages 1–7, 2016.

[4] Zhongping Lee and Shaoling Shang. Visibility: How applicable is the century-old koschmieder model? *Journal of the Atmospheric Sciences*, 73, 09 2016.

[5] Nathan Hagen. The influence of natural and artificial fogs on visible and infrared imaging. In Marija Strojnik and Maureen S. Kirk, editors, *Infrared Remote Sensing and Instrumentation XXVI*, volume 10765, pages 13 – 19. International Society for Optics and Photonics, SPIE, 2018.

[6] Hugh R. Carlon, David H. Anderson, Merrill E. Milham, Theodore L. Tarnove, Robert H. Frickel, and I. Sindoni. Infrared extinction spectra of some common liquid aerosols. *Appl. Opt.*, 16(6):1598–1605, Jun 1977.

[7] C. Osorio Quero, D. Durini, J. Rangel-Magdaleno, J. Martinez-Carranza, and R. Ramos-Garcia. Single-pixel near-infrared 3d image reconstruction in outdoor conditions. *Micromachines*, 13(5), 2022.

[8] Carlos A. Osorio Quero, Daniel Durini, Jose Rangel-Magdaleno, and Jose Martinez-Carranza. Single-pixel imaging: An overview of different methods to be used for 3d space reconstruction in harsh environments. *Review of Scientific Instruments*, 92(11):111501, 2021.

[9] Kaiming He, Jian Sun, and Xiaoou Tang. Single image haze removal using dark channel prior. In *2009 IEEE Conference on Computer Vision and Pattern Recognition*, pages 1956–1963, 2009.

[10] Xin Yang, Yang Liu, Xinyue Mou, Tianyu Hu, Fei Yuan, and En Cheng. Imaging in turbid water based on a hadamard single-pixel imaging system. *Opt. Express*, 29(8):12010–12023, Apr 2021.

[11] Graham M. Gibson, Steven D. Johnson, and Miles J. Padgett. Single-pixel imaging 12 years on: a review. *Opt. Express*, 28(19):28190–28208, Sep 2020.

[12] Zibang Zhang, Xueying Wang, Guoan Zheng, and Jingang Zhong. Hadamard single-pixel imaging versus fourier single-pixel imaging. *Opt. Express*, 25(16):19619–19639, Aug 2017.

[13] Giorgia Franchini, Roberto Cavicchioli, and Jia Cheng Hu. Stochastic floyd-steinberg dithering on gpu: image quality and processing time improved. In *2019 Fifth International Conference on Image Information Processing (ICIIP)*, pages 1–6, 2019.

[14] C. Osorio Quero, D. Durini, R. Ramos-Garcia, J. Rangel-Magdaleno, and J. Martinez-Carranza. Hardware parallel architecture proposed to accelerate the orthogonal matching pursuit compressive sensing reconstruction. In Lei Tian, Jonathan C. Petruccelli, and Chrysanthe Preza, editors, *Computational Imaging V*, volume 11396, pages 56 – 63. International Society for Optics and Photonics, SPIE, 2020.

[15] Wang Lin, Bi Du-Yan, Li Quan-He, and He Lin-Yuan. Single image dehazing based on visual-physical model. In Yu-Jin Zhang, editor, *Image and Graphics*, pages 360–368, Cham, 2015. Springer International Publishing.